Brain Tumor Segmentation of Magnetic Resonance Imaging (MRI) Images Using Deep Neural Network Driven Unmodified and Modified U-Net Architecture

Nunik Destria Arianti[1], Azah Kamilah Muda[2]*
Fakulti Teknologi Maklumat dan Komunikasi, Universiti Teknikal Malaysia Melaka, Melaka, Malaysia[1, 2]
Department of Information System, Nusa Putra University, Sukabumi, Indonesia[2]

***Abstract*—Accurately separating healthy tissue from tumorous regions is crucial for effective diagnosis and treatment planning based on magnetic resonance imaging (MRI) data. Current manual detection methods rely heavily on human expertise, so MRI-based segmentation is essential to improving diagnostic accuracy and treatment outcomes. The purpose of this paper is to compare the performance of detecting brain tumors from MRI images through segmentation using an unmodified and modified U-Net architecture from deep neural network (DNN) that has been modified by adding batch normalization and dropout on the encoder layer with and without the freeze layer. The study utilizes a public 2D brain tumor dataset containing 3064 T1-weighted contrast-enhanced images of meningioma, glioma, and pituitary tumors. Model performance was evaluated using intersection over union (IoU) and standard metrics such as precision, recall, f1-score, and accuracy across training, validation, and testing stages. Statistical analysis, including ANOVA and Duncan's multiple range test, was conducted to determine the significance of performance differences across the architectures. Results indicate that while the modified architectures show improved stability and convergence, the freeze layer model demonstrated superior IoU and efficiency, making it a promising approach for more accurate and efficient brain tumor segmentation. The comparison of the three methods revealed that the modified U-Net architecture with a freeze layer significantly reduced training time by 81.72% compared to the unmodified U-Net while maintaining similar performance across validation and testing stages. All three methods showed comparable accuracy and consistency, with no significant differences in performance during validation and testing.**

Keywords*—Accuracy; brain tumor; DNN; U-Net architecture; comparison performance

I. INTRODUCTION

Brain tumors are among the most life-threatening conditions, with the potential to drastically affect the quality of life and survival of patients. Early and accurate diagnosis is paramount to developing effective treatment strategies, often involving surgery, radiotherapy, or chemotherapy. Magnetic resonance imaging (MRI) is widely recognized as one of the most accurate non-invasive imaging techniques for detecting brain abnormalities. It provides detailed views of brain structures and tissue compositions, allowing clinicians to assess tumor size, location, and growth patterns from research in quantitative MRI [1], research review [2], and discussion from Advancements in Neuroimaging to detect brain tumors [3]. However, interpreting these MRI images is complex and time-consuming, requiring a high level of expertise [4]. As a result, manual segmentation of brain tumors can be inconsistent, subjective, and prone to human error. Automated segmentation methods using advanced machine learning and deep learning techniques have been explored to address these challenges in recent years using image cardiac radiography [5], image Alzheimer's disease in the human brain [6], and brain tumor detection using MRI [7].

Deep neural networks (DNNs), particularly convolutional neural networks (CNNs), have shown exceptional promise in image analysis tasks, including medical image segmentation. CNNs are highly effective at identifying patterns in image data by leveraging layers that automatically learn relevant features such as edges, textures, and complex structures. Among CNN-based methods, the U-Net architecture has become a leading tool for medical image segmentation due to its robust performance. Initially designed for biomedical image segmentation, U-Net uses an encoder-decoder structure, where the encoder extracts features from the input image, and the decoder uses those features to reconstruct segmented regions [8, 9]. U-Net's symmetrical architecture enables precise localization of structures, making it especially suitable for segmenting brain tumors. According to Yousef, et al. [10], despite its strengths, the standard U-Net architecture can be prone to overfitting, mainly when training on small datasets like MRI brain scans, leading to decreased generalization to unseen data.

Several improvements have been proposed to address the limitations of the original U-Net architecture, focusing on enhancing the model's generalization and stability during training. Two commonly employed techniques, batch normalization and dropout, have been used to learn parameter effects for segmenting brain tumors [11], mandible bones [12], and brain tumors using U-Net [13]. Batch normalization is used to normalize the input to each layer during training, reducing internal covariate shifts and accelerating the learning process. By stabilizing the learning process, batch normalization helps improve the performance of deep neural networks, mainly when applied to complex datasets like MRI images. On the other hand, dropout is a regularization technique that randomly disables a fraction of neurons during training, forcing the network to learn more robust features. This helps to mitigate overfitting by preventing the model

from relying too heavily on specific neurons [14]. Batch normalization and dropout can significantly enhance the U-Net architecture's ability to generalize from training data to new, unseen cases.

In addition to these regularization techniques, another modification involves freezing specific layers of the U-Net architecture during training. The freeze layer method limits the number of trainable layers, essentially "freezing" network parts to prevent them from being updated during training. This can be particularly useful when fine-tuning a model on a smaller dataset or using transfer learning [15]. By restricting the training depth, the model is less likely to overfit the specific training data and can generalize better to new data. Furthermore, freezing layers can reduce the computational cost of training, as fewer parameters need to be updated [16]. This makes it an attractive option for optimizing the training process without sacrificing performance. The combination of batch normalization, dropout, and freeze layers has the potential to significantly improve the efficiency and accuracy of brain tumor segmentation using MRI images.

The U-Net architecture, in original and with modifications in architecture, remains one of the most widely used models for medical image segmentation tasks. The original U-Net is effective but may struggle with specific challenges inherent to brain tumor segmentation, such as distinguishing between subtle boundaries of healthy and tumorous tissues [8]. Incorporating batch normalization and dropout into the encoder layers enhances the model's ability to avoid overfitting, allowing it to learn more generalized features. Furthermore, introducing a freeze layer can optimize computational efficiency, making the model more robust and faster to train. These architectural improvements hold great promise for improving the segmentation of brain tumors, ultimately contributing to better diagnostic accuracy and treatment planning.

This paper compares the performance of brain tumor segmentation using unmodified and modified U-Net architectures driven by deep neural networks (DNN). Specifically, two modifications are examined: (1) batch normalization and dropout added to the encoder layer, and (2) a freeze layer introduced to limit the depth of the training process. We selected the modified U-Net architecture with batch normalization, dropout, and freeze layers due to its effectiveness in addressing specific challenges in brain tumor segmentation. U-Net, widely used in medical image segmentation, excels at delineating complex structures, but it can struggle with overfitting, particularly on small datasets like MRI. To mitigate this, batch normalization stabilizes training by normalizing layer inputs, while dropout prevents over-reliance on specific neurons, reducing overfitting. Additionally, freeze layers limit trainable parameters, improving generalization and reducing computational cost. Standard methods often fail to handle subtle tumor boundaries and are prone to overfitting with small datasets. Our modifications enhance the model's robustness, efficiency, and accuracy in segmenting brain tumors. These improvements address limitations in existing approaches, making our method more suitable for the complexities of brain tumor segmentation from MRI images, where precise and reliable detection is critical.

The remainder of this paper is structured as follows: Section II overviews brain tumor segmentation using deep learning as a related work. Section III explains the dataset and methods in detail. In Section IV, we compare and analyze experiments and discussions from our studies. Finally, Section V concludes and describes future work.

II. Related Work

Research on brain tumor segmentation using deep learning has gained substantial attention in recent years due to the increasing availability of medical imaging data and the advancements in computational methods. Early approaches to brain tumor segmentation relied heavily on traditional image processing techniques such as thresholding, region growing, and edge detection [17-19]. While these methods could detect certain features, they lacked the sophistication needed to capture brain tumors' complex and heterogeneous nature. As a result, their accuracy was often limited, especially when dealing with tumors with irregular shapes or indistinct boundaries. The development of machine learning models, particularly convolutional neural networks (CNNs), revolutionized this field by enabling more automated, accurate, and efficient segmentation techniques, especially in medical imaging applications such as brain tumor detection.

One of the first major breakthroughs in deep learning-based medical image segmentation came with the introduction of the U-Net architecture by Ronneberger, et al. [20]. Initially designed for biomedical image segmentation tasks, U-Net rapidly gained popularity due to its simplicity and effectiveness. The architecture's encoder-decoder structure enables precise segmentation by combining high-resolution features from the encoder with upsampled features in the decoder. U-Net has been successfully applied to various medical imaging tasks, including brain tumor segmentation, and has become a standard baseline model in the field. However, despite its success, U-Net often struggles with overfitting and performance stability, mainly when dealing with minor or imbalanced datasets, which are common in medical imaging.

Various enhancements to the U-Net architecture have been proposed to address these issues. Isensee, et al. [21] introduced modifications such as deep supervision and residual connections to improve the network's ability to learn from complex medical imaging data. Other works have focused on regularization techniques like batch normalization and dropout to enhance model stability and generalization. Batch normalization, introduced by Ioffe [22], is commonly used to normalize the inputs to each layer, speeding up training and reducing internal covariate shifts. Dropout, proposed by Srivastava, et al. [23], helps prevent overfitting by randomly deactivating neurons during training, forcing the model to learn more generalized features. Various CNN architectures, including U-Net, have widely adopted these techniques to improve their performance on medical image segmentation tasks.

Additionally, several researchers have explored transfer learning and fine-tuning in medical image segmentation. Transfer learning allows a pre-trained model to be adapted to a new task by freezing specific layers during training and updating only a subset of parameters. In brain tumor segmentation, transfer learning can be particularly beneficial when working with small datasets, as it enables models to leverage knowledge from larger, more general datasets. Kamnitsas, et al. [24] demonstrated the effectiveness of transfer learning for brain lesion segmentation using a 3D CNN, achieving better performance than training from scratch. The use of freeze layers, which limit the depth of training, has also been explored to reduce overfitting and optimize computational efficiency, particularly in resource-constrained environments.

Moreover, ensemble learning methods have been explored to improve segmentation performance further. DeepMedic, introduced by Kamnitsas, et al. [25], combines multiple CNNs to form an ensemble model, resulting in more robust and accurate brain tumor segmentation. Other works have integrated different architectures, such as residual networks and attention mechanisms, to enhance segmentation models' feature extraction and localization capabilities. In summary, the field of brain tumor segmentation has seen significant advancements, with numerous modifications to the original U-Net architecture and the incorporation of advanced techniques such as batch normalization, dropout, freeze layers, and ensemble learning approaches. These improvements enhance model stability, reduce overfitting, and increase segmentation accuracy.

III. Dataset and Methods

A. Data Sets

The dataset used in this study is a public 2D brain tumor dataset authored by Cheng, et al. [26], Cheng, et al. [27]. The dataset contains 3064 T1-weighted contrast-enhanced images with three kinds of brain tumors (meningioma with 708 slices, glioma with 1426 slices, and pituitary tumor with 930 slices) from 233 patients that were scanned by magnetic resonance imaging (MRI), all with ground truth segmentations of the tumors. It was randomly split into a training set of 2451 images, an internal validation set of 306 images, and a testing set of 307 images.

B. The Proposed Method

In this study, three architectures from deep neural network (DNN) were used, including (1) an unmodified U-Net architecture, (2) a modified U-Net architecture with batch normalization and dropout on the encoder layer without the freeze layer, and (3) a modified U-Net architecture with batch normalization and dropout on the encoder layer with a freeze layer. The U-Net architecture added with freeze layers aims to limit the training depth by skipping certain layers when training the model.

C. Evaluation of the Models Performance

During the calibration stages (training and internal validation) for the three architectures examined in this study, the performance of the model development is evaluated through training loss and validation loss. Moreover, as a widely-used evaluation metric in object detection and image segmentation tasks, the intersection over union (IoU) overlap between predicted bounding boxes and ground truth boxes is also evaluated with scores ranging from 0 to 1. After that, the model is tested using a dataset of 307 images.

To find out more details regarding the model performance of each stages (training, internal validation, testing), 10 images were randomly taken from each stages to be compared to the ground truth segmentations of the tumors. Each image will be checked for the number of true positive, true negative, false negative, and false positive variables to calculate precision, recall, f1-score, and accuracy. After that, the average with the standard deviation for the three architectures was compared through the ANOVA statistical test to determine the model performance's significance ($p<0.05$). Duncan's multiple range test will be carried out if at least one difference exists between the three architectures.

IV. Result and Discussions

A. Unmodified U-Net Architecture

Fig. 1(a) shows the training history for 35 epochs using unmodified U-Net architecture for the loss training (0.1453±1.21E-01) and internal validation (0.1931±5.10E-02) stages. There is a loss gap of around 32.94% between training and validation. The loss curve for validation shows that the best loss can be achieved at an epoch of 35. The time calculation for running training for this method is 197.11±0.37s. The performance of the model by the intersection of union (IoU) on Fig. 1(b) for unmodified U-Net architecture is 0.7376±1.41E-01 in training and 0.6861±2.92E-02 in validation. There is a difference in IoU of approximately 6.98% between the training and validation results.

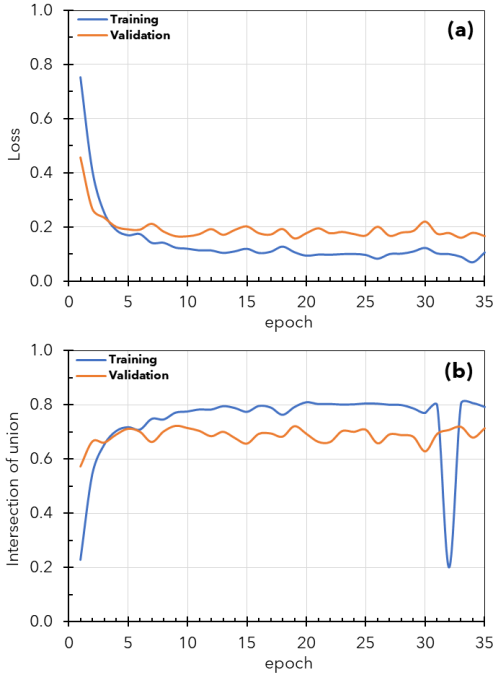

Fig. 1. Training and validation history of 35 epochs iteration from unmodified U-Net architecture model (a) accuracy and (b) IoU.

Fig. 2 presents the model's performance when sampling 10 images for the confusion matrix. The model from unmodified U-Net is more accurate (Fig. 2(a)) than the validation and testing stages except in images number 4, 5, and 7 (see Fig. 3). The average accuracy at the training, validation, and testing steps were 0.9977+7.46E-04, 0.9979+7.27E-04, and 0.9979+1.18E-03, respectively. The ANOVA test results for the accuracy parameters at the training, validation, and testing steps were not significantly different (p>0.05), indicating that the model is steady and there is no under/overfitting.

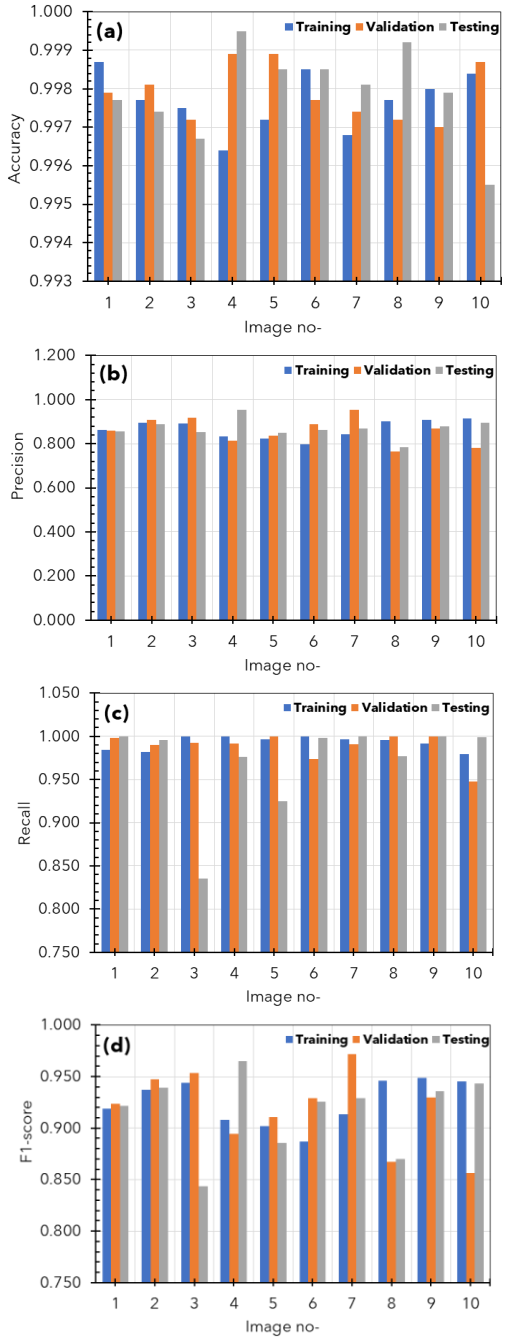

Fig. 2. Performance of sampling image from unmodified U-Net in a confusion matrix (a) accuracy, (b) precision, (c) recall and (d) f1-score.

Precision can be used as a parameter to measure how consistent the model is in predicting the quality of positive predictions. The average precision (see Fig. 2(b)) at the training, validation, and testing stages were 0.8670+4.12E-02, 0.8593+6.04E-02, and 0.8685+4.27E-02, respectively. The statistical test results using ANOVA did not find any significant differences between the three stages (p>0.05). This indicates that the results obtained through precision did not find any false patterns from the tested dataset.

Next, the recall parameter can show the total number of actual positive cases that are correctly predicted to show the sensitivity of the model. The average recall (Fig. 2(c)) at the training, validation, and testing stages are 0.9927+7.95E-03, 0.9884+1.63E-02, and 0.9706+5.30E-02, respectively. The ANOVA statistical test results revealed no significant differences across the three stages (p>0.05), indicating that the recall results did not detect incorrect patterns in the tested dataset.

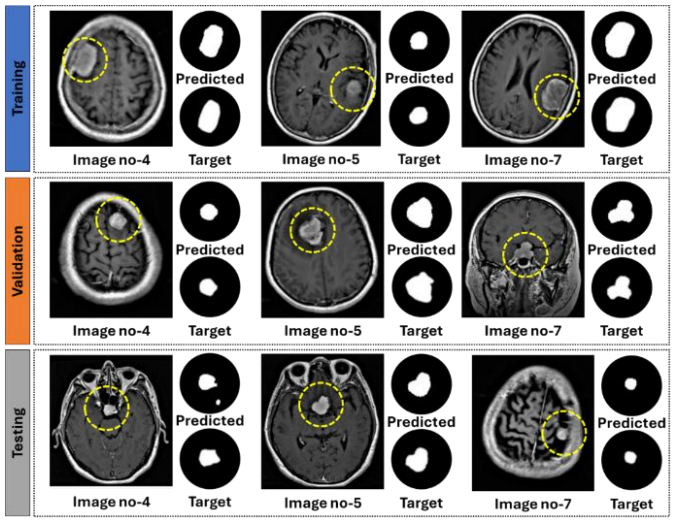

Fig. 3. Details of sample images 4, 5, and 7 in training, validation, and testing by unmodified U-Net architecture model.

B. Modified U-Net Architecture without Freeze Layer

The training and validation history and IoU for 35 epochs using modified U-Net architecture without a freeze layer are depicted in Fig. 4. The training and internal validation loss are 0.2778±5.70E-02 and 0.2927±5.01E-02, respectively. There is a loss gap of around 5.37% between training and validation. The loss curve for validation shows that the best accuracy can be achieved at an epoch of 35. The time required for running the training with this method is 55.66±0.48s. The model's performance, measured by the intersection over union (IoU), for the modified U-Net architecture without a frozen layer is 0.5633±7.15E-02 during training and 0.5591±5.69E-02 during validation. The IoU difference between the training and validation results is approximately 0.74%.

The confusion matrix in Fig. 5 shows the performance of the modified U-Net architecture without the frozen layer, based on sampling 10 images. As depicted in Fig. 5(a), the model maintains stability in all stages, except image sample number 3, where a deviation in accuracy is observed (Fig. 6). The average accuracy during the training, validation, and

testing stages was 0.9951±2.92E-03, 0.9929±8.08E-03, and 0.9865±2.96E-02, respectively. The ANOVA test results showed no significant differences (p>0.05) in accuracy across these stages, implying that the model is steady and does not exhibit underfitting or overfitting.

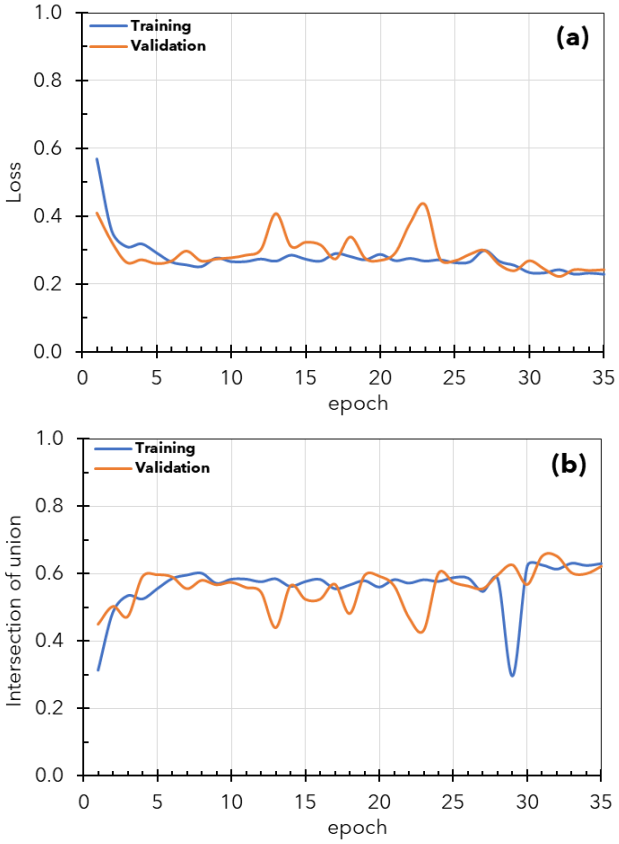

Fig. 4. Training and validation history of 35 epochs iteration from modified U-Net architecture without freeze layer model (a) accuracy and (b) IoU.

Precision as a key parameter for evaluating the model's consistency in predicting positive outcomes, yielded average scores of 0.7883±7.77E-02, 0.7511±2.04E-01, and 0.7592±2.18E-01 during the training, validation, and testing stages, respectively (Fig. 5(b)). Similarly, recall that measures the model's sensitivity in correctly predicting actual positive cases showed average values of 0.9784±5.25E-02, 0.8883±1.94E-01, and 0.8018±2.58E-01 across the same stages (Fig. 5(c)). Finally, the f1-Score, which balances precision and recall, averaged 0.8695±4.12E-02, 0.8029±1.82E-01, and 0.7584±2.21E-01 (Fig. 5(d)). An ANOVA analysis of these metrics (Precision, recall, and f1-Score) revealed no significant differences between the training, validation, and testing stages (p>0.05), indicating no false or incorrect patterns were identified in the dataset.

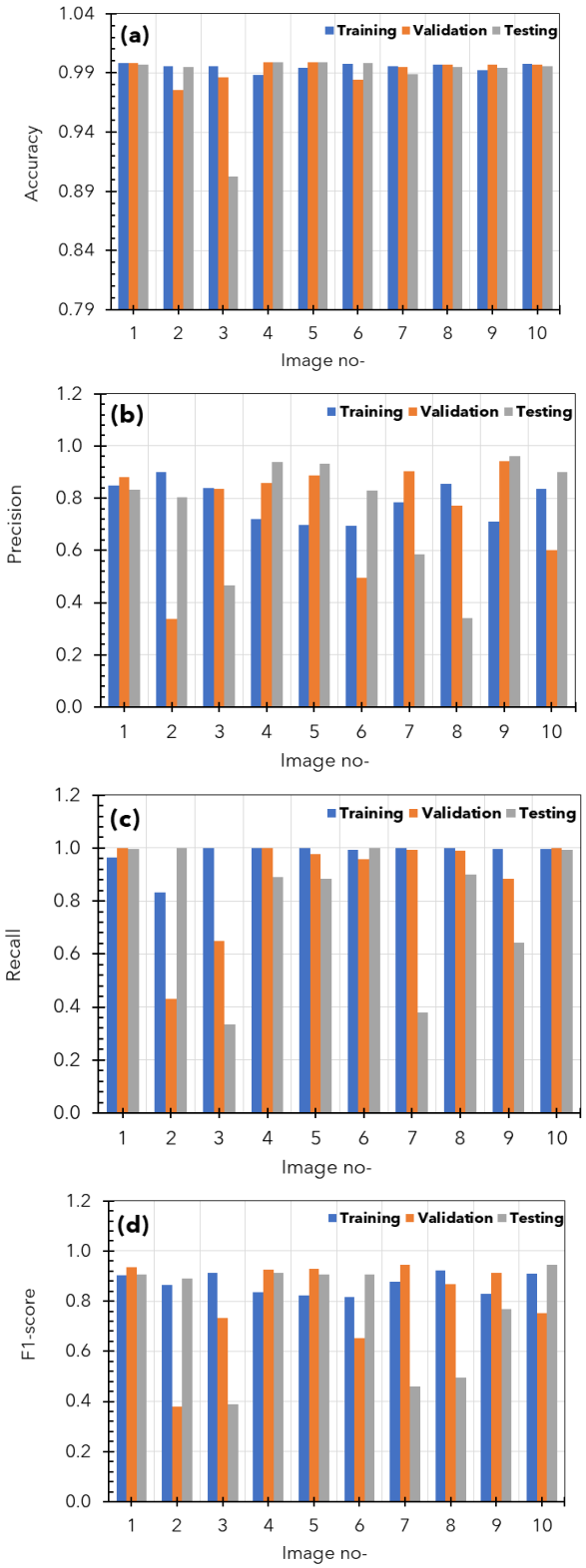

Fig. 5. Performance of sampling image from modified U-Net architecture without freeze in a confusion matrix (a) accuracy, (b) precision, (c) recall and (d) f1-score.

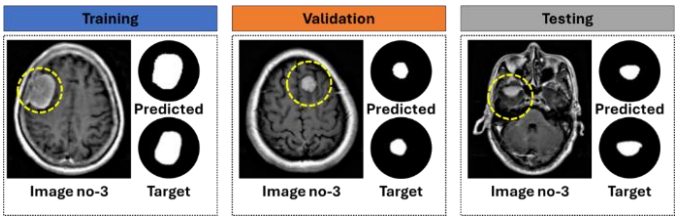

Fig. 6. Details of sample images 3 in training, validation, and testing by modified U-Net architecture without freeze model.

C. Modified U-Net Architecture with Freeze Layer

Fig. 7(a) illustrates the training history over 35 epochs using the modified U-Net architecture with a frozen layer, showing a training loss of 0.1947±7.71E-02 and a validation loss of 0.2468±3.86E-02. The loss difference between training and validation is approximately 26.73%. The training runtime for this method is calculated at 36.03±0.17s. Fig. 7(b) presents the model's performance, with an intersection over union (IoU) of 0.6764±8.10E-02 for training and 0.5995±5.14E-02 for validation, resulting in a 11.37% IoU difference between training and validation.

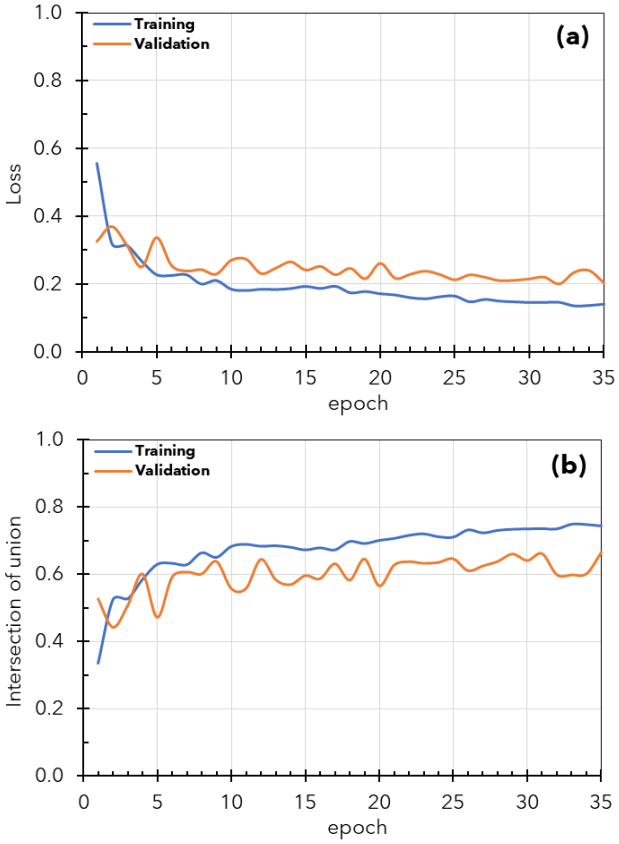

Fig. 7. Training and validation history of 35 epochs iteration from modified U-Net architecture with freeze layer model (a) accuracy and (b) IoU.

The confusion matrix in Fig. 8 illustrates the performance of the modified U-Net architecture with the frozen layer based on a sample of 10 images. As illustrated in Figure 8a, the model demonstrates stability across all stages, except image sample numbers 2 and 3, where a decline in validation accuracy is observed, and image sample number 5 shows a decrease in precision during the testing stage (Fig. 9). The average accuracy during the training, validation, and testing stages was 0.9973±1.35E-03, 0.9942±7.68E-03, and 0.9949±4.50E-03, respectively. ANOVA test results indicated that the model is stable and does not exhibit indications of underfitting or overfitting, as there were no significant differences in accuracy between these stages (p>0.05).

During the training, validation, and testing stages, the average precision scores for predicting favorable outcomes were 0.8742±5.43E-02, 0.8251±1.82E-01, and 0.6831±3.85E-01, respectively (Fig. 8(b)). Conversely, the recall metric, which quantifies the model's ability to accurately anticipate real positive instances, had mean values of 0.9549±6.05E-02, 0.8348±2.66E-01, and 0.8146±3.03E-01 over the same stages (Fig. 8(c)). In Fig. 8(d), the f1-Score, which measures the balance between accuracy and recall, had average values of 0.9109±3.92E-02, 0.8120±2.10E-01, and 0.7022±3.83E-01. Statistical study of the metrics (precision, recall, and f1-Score) using ANOVA showed no statistically significant variations throughout the training, validation, and testing stages (p>0.05). This suggests no erroneous or inaccurate patterns were detected in the dataset.

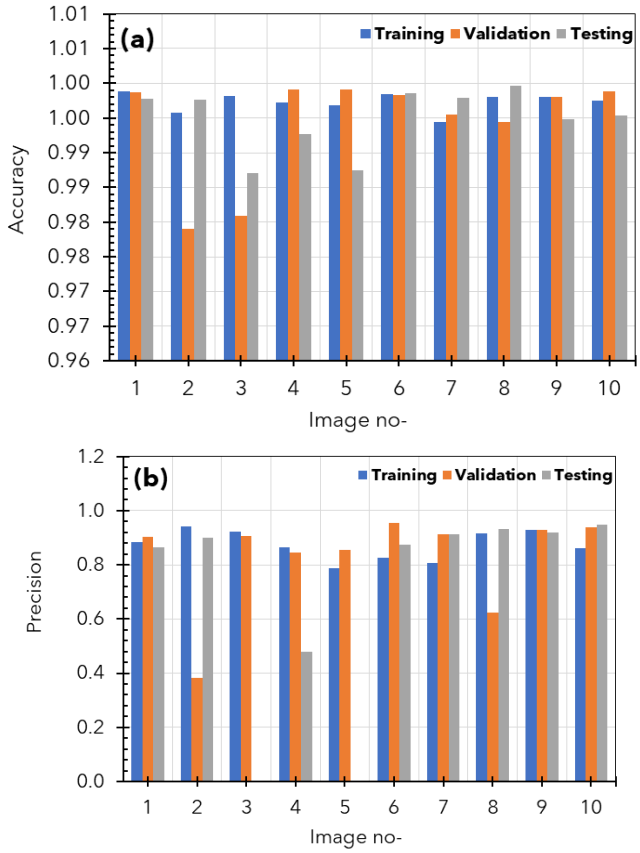

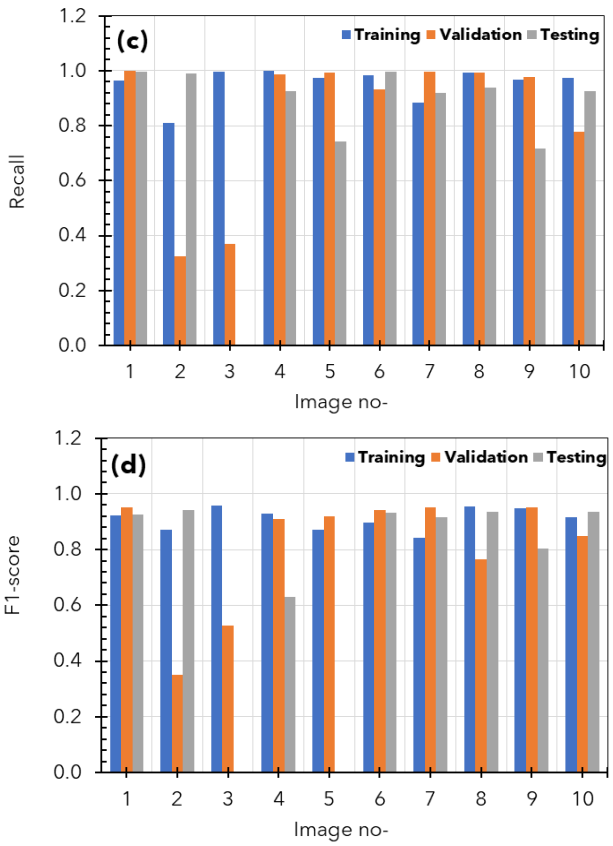

Fig. 8. Performance of sampling image from modified U-Net architecture with freeze in a confusion matrix (a) accuracy, (b) precision, (c) recall and (d) f1-score.

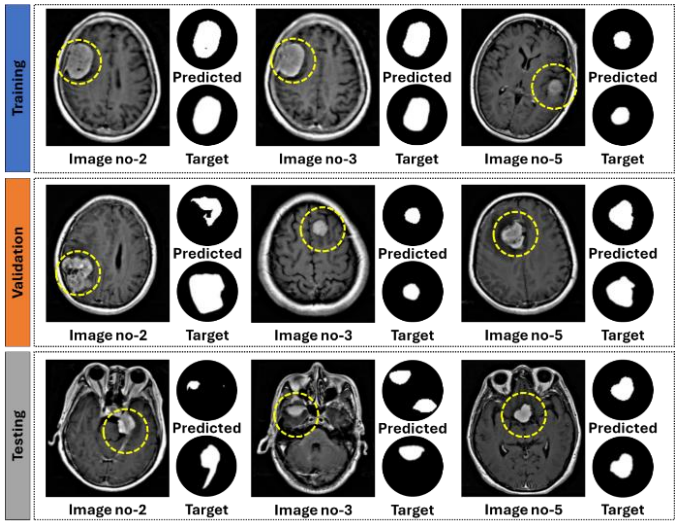

Fig. 9. Details of sample images 3 in training, validation, and testing by modified U-Net architecture with freeze model.

D. Comparison Performance Between the Proposed Method

The performance comparison of the three methods used in this study at each modeling stage is presented in Fig. 10. It can be seen that at the training stage for all parameters, there is a significant difference (p<0.05) between the three methods tested except for the recall parameter. However, no difference in performance was found between the three methods for the validation and testing stages (p>0.05). Finally, the method with modified U-net architecture with a freeze layer provides a significant difference in training time calculation. Meanwhile, the model performance is equally suitable for all three using unmodified U-Net architecture. Therefore, the method proposed through this study that combines modified U-net architecture with a freeze layer provides a more efficient calculation time efficiency of around 83% than unmodified U-net architecture. Compared with previous research, as reported by Cheng, et al. [26], this study's results have been better than those of prior research, as presented in Fig. 10(e).

The practical motivation for applying the theoretical results obtained in this study lies in improving the accuracy and efficiency of brain tumor segmentation in clinical settings. Accurate segmentation is crucial for diagnosing, planning treatment, and monitoring tumor progression, yet manual segmentation is time-consuming and prone to variability. Our modified U-Net architecture, enhanced with batch normalization, dropout, and freeze layers, offers a robust and scalable solution that addresses common issues such as overfitting and computational inefficiency, mainly when working with small MRI datasets. These theoretical improvements translate into more reliable, faster, and precise automated segmentation, ultimately aiding clinicians in making more informed decisions. The ability to generalize across different cases ensures that the model can be applied in real-world medical environments, improving diagnostic workflows and potentially leading to better patient outcomes through more personalized and accurate treatment strategies.

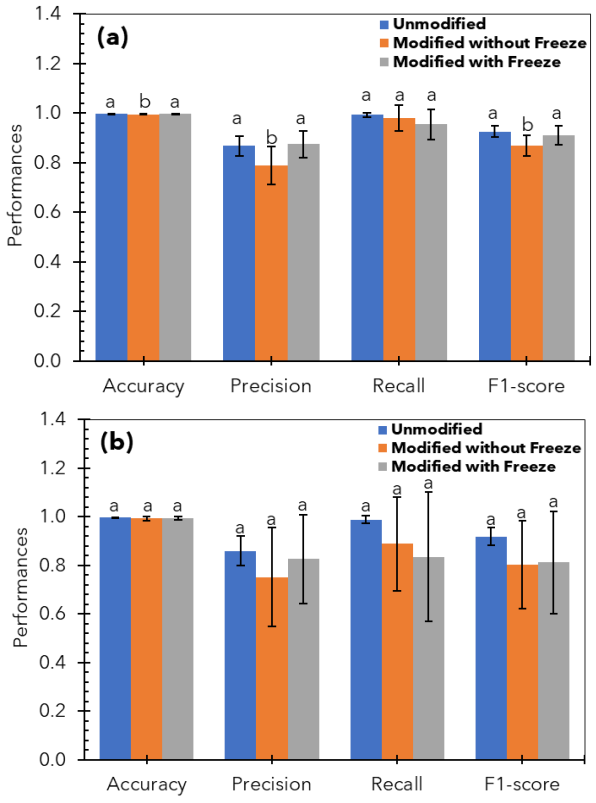

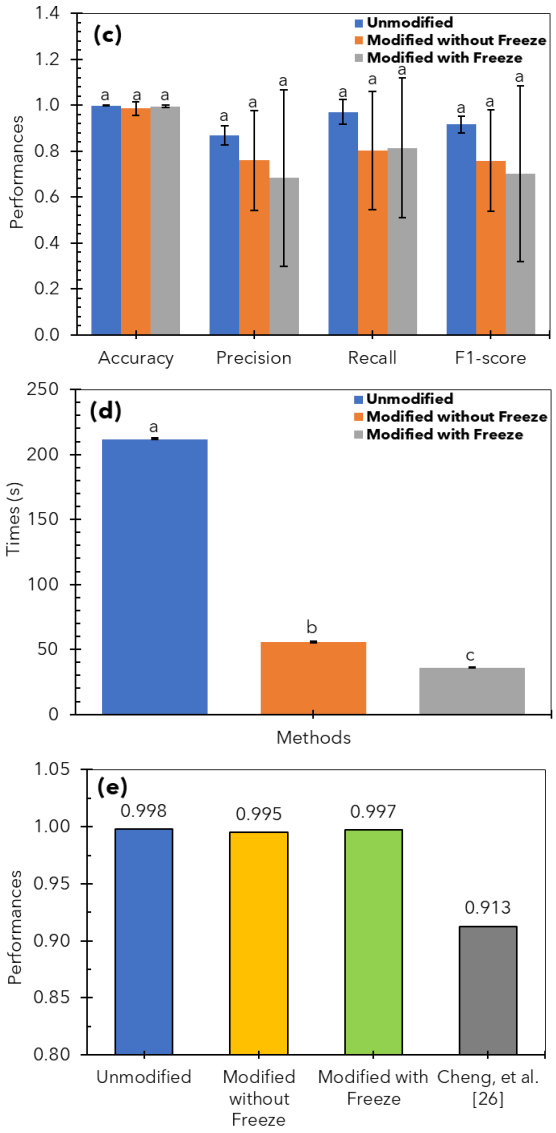

Fig. 10. Comparison performance between the proposed method on (a) training, (b) validation, (c) testing, (d) times and (e) comparison with a result from [26].

V. Conclusions and Future Work

In this study, we compared the performance of unmodified and modified U-Net architectures for brain tumor segmentation from MRI images, focusing on enhancements through batch normalization, dropout, and freeze layers. While the unmodified U-Net provided reliable performance, it exhibited a slight loss gap between training and validation, hinting at potential overfitting and resulting in lower intersection over union (IoU) scores. On the other hand, the modified U-Net without a freeze layer demonstrated improved convergence and reduced loss, with higher IoU scores indicating better segmentation capabilities. However, some inconsistencies were observed in precision and recall during the testing stage, showing that further optimization was necessary while the modifications improved performance. The most promising results came from the modified U-Net with a freeze layer, which achieved the highest IoU scores and maintained stability across all performance metrics, including accuracy, precision, recall, and f1-score. This model effectively mitigated overfitting by limiting the training depth while reducing the computational time required, making it highly efficient for practical use. The freeze layer modification proved particularly beneficial, allowing for a balance between model complexity and computational efficiency.

The modified U-Net architecture with a freeze layer significantly reduced training time by 81.72% compared to the unmodified U-Net while maintaining similar performance across validation and testing stages. Despite the differences observed in training, all three methods performed equally well regarding segmentation accuracy and consistency. While the unmodified U-Net is a solid baseline for segmentation tasks, the modified U-Net, especially with the freeze layer, shows superior performance, making it more suitable for real-world applications where accuracy and efficiency are paramount. Future studies could investigate further improvements to these architectures by incorporating advanced optimization methods and expanding the dataset to include more diverse tumor types and imaging conditions, thereby enhancing the model's generalizability.

References

[1] N. Weiskopf, L. J. Edwards, G. Helms, S. Mohammadi, E. Kirilina. Quantitative magnetic resonance imaging of brain anatomy and in vivo histology. Nature Reviews Physics. 2021. 3(8): 570-588.

[2] M. Martucci, R. Russo, F. Schimperna, G. D'Apolito, M. Panfili, A. Grimaldi, A. Perna, A. M. Ferranti, G. Varcasia, C. Giordano. Magnetic resonance imaging of primary adult brain tumors: state of the art and future perspectives. Biomedicines. 2023. 11(2): 364.

[3] F. Sanvito, A. Castellano, A. Falini. Advancements in neuroimaging to unravel biological and molecular features of brain tumors. Cancers. 2021. 13(3): 424.

[4] H. Saleem, A. R. Shahid, B. Raza. Visual interpretability in 3D brain tumor segmentation network. Computers in Biology and Medicine. 2021. 133: 104410.

[5] Y. Song, S. Ren, Y. Lu, X. Fu, K. K. Wong. Deep learning-based automatic segmentation of images in cardiac radiography: a promising challenge. Computer Methods and Programs in Biomedicine. 2022. 220: 106821.

[6] N. Yamanakkanavar, J. Y. Choi, B. Lee. MRI segmentation and classification of human brain using deep learning for diagnosis of Alzheimer's disease: a survey. Sensors. 2020. 20(11): 3243.

[7] M. Mittal, M. Arora, T. Pandey, L. M. Goyal. Image segmentation using deep learning techniques in medical images. Advancement of machine intelligence in interactive medical image analysis. 2020. 41-63.

[8] N. S. Punn, S. Agarwal. Modality specific U-Net variants for biomedical image segmentation: a survey. Artificial Intelligence Review. 2022. 55(7): 5845-5889.

[9] R. Azad, E. K. Aghdam, A. Rauland, Y. Jia, A. H. Avval, A. Bozorgpour, S. Karimijafarbigloo, J. P. Cohen, E. Adeli, D. Merhof. Medical image segmentation review: The success of u-net. IEEE Transactions on Pattern Analysis and Machine Intelligence. 2024.

[10] R. Yousef, S. Khan, G. Gupta, T. Siddiqui, B. M. Albahlal, S. A. Alajlan, M. A. Haq. U-Net-based models towards optimal MR brain image segmentation. Diagnostics. 2023. 13(9): 1624.

[11] S. Das, M. k. Swain, G. K. Nayak, S. Saxena, S. Satpathy. Effect of learning parameters on the performance of U-Net Model in segmentation of Brain tumor. Multimedia tools and applications. 2022. 81(24): 34717-34735.

[12] N. Talat, A. Alsadoon, P. Prasad, A. Dawoud, T. A. Rashid, S. Haddad. A novel enhanced normalization technique for a mandible bones

segmentation using deep learning: batch normalization with the dropout. Multimedia Tools and Applications. 2023. 82(4): 6147-6166.

[13] M. U. Rehman, S. Cho, J. H. Kim, K. T. Chong. Bu-net: Brain tumor segmentation using modified u-net architecture. Electronics. 2020. 9(12): 2203.

[14] B. Lengerich, E. P. Xing, R. Caruana. On dropout, overfitting, and interaction effects in deep neural networks. arXiv preprint arXiv:2007.00823. 2020. 2.

[15] R. K. Samala, H.-P. Chan, L. M. Hadjiiski, M. A. Helvie, C. D. Richter. Generalization error analysis for deep convolutional neural network with transfer learning in breast cancer diagnosis. Physics in Medicine & Biology. 2020. 65(10): 105002.

[16] M. Iman, H. R. Arabnia, K. Rasheed. A review of deep transfer learning and recent advancements. Technologies. 2023. 11(2): 40.

[17] P. Jyothi, A. R. Singh. Deep learning models and traditional automated techniques for brain tumor segmentation in MRI: a review. Artificial intelligence review. 2023. 56(4): 2923-2969.

[18] T. A. Soomro, L. Zheng, A. J. Afifi, A. Ali, S. Soomro, M. Yin, J. Gao. Image segmentation for MR brain tumor detection using machine learning: a review. IEEE Reviews in Biomedical Engineering. 2022. 16: 70-90.

[19] J. Ramasamy, R. Doshi, K. K. Hiran, "Segmentation of brain tumor using deep learning methods: a review," in Proceedings of the International Conference on Data Science, Machine Learning and Artificial Intelligence, 2021, pp. 209-215.

[20] O. Ronneberger, P. Fischer, T. Brox, "U-net: Convolutional networks for biomedical image segmentation," in Medical image computing and computer-assisted intervention–MICCAI 2015: 18th international conference, Munich, Germany, October 5-9, 2015, proceedings, part III 18, 2015: Springer, pp. 234-241.

[21] F. Isensee, P. Kickingereder, W. Wick, M. Bendszus, K. H. Maier-Hein, "No New-Net," in Brainlesion: Glioma, Multiple Sclerosis, Stroke and Traumatic Brain Injuries, Cham, 2019: Springer International Publishing, pp. 234-244.

[22] S. Ioffe. Batch normalization: Accelerating deep network training by reducing internal covariate shift. arXiv preprint arXiv:1502.03167. 2015.

[23] N. Srivastava, G. Hinton, A. Krizhevsky, I. Sutskever, R. Salakhutdinov. Dropout: a simple way to prevent neural networks from overfitting. The journal of machine learning research. 2014. 15(1): 1929-1958.

[24] K. Kamnitsas, C. Ledig, V. F. Newcombe, J. P. Simpson, A. D. Kane, D. K. Menon, D. Rueckert, B. Glocker. Efficient multi-scale 3D CNN with fully connected CRF for accurate brain lesion segmentation. Medical image analysis. 2017. 36: 61-78.

[25] K. Kamnitsas, W. Bai, E. Ferrante, S. McDonagh, M. Sinclair, N. Pawlowski, M. Rajchl, M. Lee, B. Kainz, D. Rueckert, "Ensembles of multiple models and architectures for robust brain tumour segmentation," in Brainlesion: Glioma, Multiple Sclerosis, Stroke and Traumatic Brain Injuries: Third International Workshop, BrainLes 2017, Held in Conjunction with MICCAI 2017, Quebec City, QC, Canada, September 14, 2017, Revised Selected Papers 3, 2018: Springer, pp. 450-462.

[26] J. Cheng, W. Huang, S. Cao, R. Yang, W. Yang, Z. Yun, Z. Wang, Q. Feng. Enhanced performance of brain tumor classification via tumor region augmentation and partition. PloS one. 2015. 10(10): e0140381.

[27] J. Cheng, W. Yang, M. Huang, W. Huang, J. Jiang, Y. Zhou, R. Yang, J. Zhao, Y. Feng, Q. Feng. Retrieval of brain tumors by adaptive spatial pooling and fisher vector representation. PloS one. 2016. 11(6): e0157112.